# ACCEPTED VERSION

Long Yu, Gleb E. Yakubov, Wei Zeng, Xiaohui Xing, John Stenson, Vincent Bulone, Jason R. Stokes

**Multi-layer mucilage of Plantago ovata seeds: Rheological differences arise from variations in arabinoxylan side chains**

Final publication at http://dx.doi.org/10.1016/j.carbpol.2017.02.038

---

**PERMISSIONS**

https://www.elsevier.com/about/our-business/policies/sharing

## Accepted Manuscript

Authors can share their accepted manuscript:

[…]

**After the embargo period**

- via non-commercial hosting platforms such as their institutional repository
- via commercial sites with which Elsevier has an agreement

**In all cases accepted manuscripts should:**

- link to the formal publication via its DOI
- bear a CC-BY-NC-ND license – this is easy to do, click here to find out how
- if aggregated with other manuscripts, for example in a repository or other site, be shared in alignment with our hosting policy
- not be added to or enhanced in any way to appear more like, or to substitute for, the published journal article

**Embargo**

**5 June 2018**

---

http://hdl.handle.net/2440/103482

# Accepted Manuscript

Title: Multi-layer mucilage of *Plantago ovata* seeds:
Rheological differences arise from variations in arabinoxylan
side chains

Authors: Long Yu, Gleb E. Yakubov, Wei Zeng, Xiaohui Xing,
John Stenson, Vincent Bulone, Jason R. Stokes

Please cite this article as: Yu, Long., Yakubov, Gleb E., Zeng, Wei., Xing, Xiaohui.,
Stenson, John., Bulone, Vincent., & Stokes, Jason R., Multi-layer mucilage of
Plantago ovata seeds: Rheological differences arise from variations in arabinoxylan
side chains.*Carbohydrate Polymers* http://dx.doi.org/10.1016/j.carbpol.2017.02.038

# Multi-layer mucilage of *Plantago ovata* seeds: Rheological differences arise from variations in arabinoxylan side chains

## Authors:

Long Yu[1], Gleb E. Yakubov[1]*, Wei Zeng[2], Xiaohui Xing[3,4], John Stenson[5], Vincent Bulone[3,4], Jason R. Stokes[1].

1. Australian Research Council Centre of Excellence in Plant Cell Walls, School of Chemical Engineering, The University of Queensland, Brisbane QLD 4076, Australia

2. Australian Research Council Centre of Excellence in Plant Cell Walls, School of BioScience, The University of Melbourne, Parkville, VIC 3010, Australia

3. Division of Glycoscience, Royal Institute of Technology (KTH), School of Biotechnology, AlbaNova University Centre, Stockholm, SE-10691, Sweden

4. Australian Research Council Centre of Excellence in Plant Cell Walls, School of Agriculture, Food and Wine, The University of Adelaide, Waite Campus, Urrbrae SA 5064, Australia

5. Malvern Instruments, Malvern, Worcestershire, WR14 1XZ, UK

Graphical abstract



1
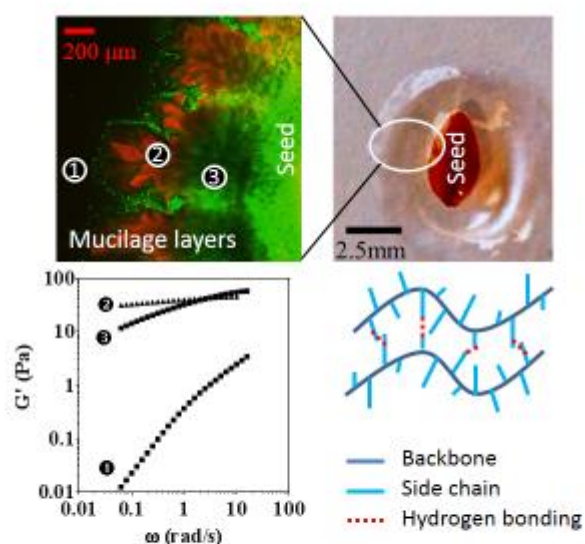
**Highlights**

- A three layered structure in *Plantago ovata* seed mucilage has been discovered.
- Major constituent arabinoxylans in each layer were isolated by step-wise extraction.
- Distinct polymer conformations were found in the structures with similar branching.
- Small differences in fine structure lead to substantial rheological differences.

## Abstract

Mucilages are hydrocolloid solutions produced by plants for a variety of functions, including the creation of a water-holding barrier around seeds. Here we report our discovery of the formation of three distinct mucilage layers around *Plantago ovata* seeds upon their hydration. Each layer is dominated by different arabinoxylans (AXs). These AXs are unusual because they are highly branched and contain β-1,3-linked xylose in their side chains. We show that these AXs have similar monosaccharide and linkage composition, but vary in their polymer conformation. They also exhibit distinct rheological properties in aqueous solution, despite analytical techniques including NMR showing little difference between them. Using enzymatic hydrolysis and chaotropic solvents, we reveal that hydrogen bonding and side chain distribution are key factors underpinning the distinct rheological properties of these complex AXs.

## Introduction

Mucilage polysaccharides are fascinating plant hydrocolloids, which help seeds to maintain hydration and survive in arid conditions or in locations where weather patterns are unstable (Huang, Boubriak, Osborne, Dong, & Gutterman, 2008). The adhesion and friction properties of the hydrated mucilage also contribute to its function in seed dispersal (Kreitschitz, Kovalev, & Gorb, 2015) and interaction with the soil (Yang, Baskin, Baskin, & Huang, 2012). However, the knowledge of the structure and gelation mechanisms in mucilage polysaccharides is limited. This is due to the complex architecture and heterogeneity of the constituent polysaccharides that typically exhibit large molecular weights in excess of 1 MDa. Seed mucilages can be broadly classified into two classes: pectin-rich and hemicellulose-rich. The pectin-rich mucilages are relatively well-studied, as illustrated by advances in characterisation of production and extrusion mechanisms in the model plant *Arabidopsis thaliana* (Griffiths et al., 2015). By contrast, a more diverse group of hemicellulosic counterparts and their constituent macromolecules remain largely unexplored, despite them being much sought-after materials for applications in drug delivery, tissue engineering and food structuring (Sun, Wang, Jing, & Mohanathas, 2013). In this work, we focus on the structure and rheological properties of the hemicellulose mucilage from *Plantago ovata* seeds (also called *psyllium*). Primary constituents of this mucilage are arabinoxylans that consist of a xylan backbone densely decorated with a variety of side chains comprised typically of xylose and arabinose residues. The structures elucidated allow the classification of these arabinoxylans as comb-like polymers.

Arabinoxylan (AX) is one of the main non-starchy polysaccharide in plants with a pivotal role in cell wall structure and assembly (Cui, 2000; Ishii, 1997; Vorwerk, Somerville, & Somerville, 2004). Ubiquitous in cereals, AXs are of major significance in human nutrition as readily fermentable substrates for gut microbiota (Broekaert et al., 2011). In addition, uncharged AXs have proven themselves useful within a diverse spectrum of industrial applications ranging from emulsification, gel structuring and rheology modification (Niño-Medina et al., 2009; Yadav et al., 2016). The formation of gels from AX is typically via covalent cross-links formed between ferulic acid residues of neighbouring α-L-Ara*f* side chains (Carvajal-Millan et al., 2005; Niño-Medina et al., 2010). In addition, such factors as molecular weight, the Ara/Xyl ratio and the degree of branching have direct impact on the rheological properties of AX-based hydrogels (Höije, Sternemalm, Heikkinen, Tenkanen, & Gatenholm, 2008; M. S. Izydorczyk & Biliaderis, 1995).

AXs are typically composed of a 1,4-linked-β-D-Xyl*p* backbone to which α-L-Ara*f* substituents are attached at the 2 and 3 positions (Izydorczyk & Dexter, 2008). Compared to their wheat-derived counterparts, the AXs from *P. ovata* seed mucilage appear to occupy a unique niche in terms of their highly branched structure and unusual linkage composition. Another similarly highly branched arabinoxylan was recently identified in leaf bases of New Zealand flax (Centanni et al., 2017; Sims & Newman, 2006). A number of possible structures have been proposed for the backbone as well as side-chains. Current data consensually favour a β-(1,4)-linked D-Xyl*p* backbone with a broad variation of the side chains and substituents attached in O-2 and/or O-3 positions (Edwards, Chaplin, Blackwood, & Dettmar, 2003; Fischer et al., 2004; Kennedy, Sandhu, & Southgate, 1979; Sandhu, Hudson, & Kennedy, 1981). The side chains and substituents include mono-substitution with α-L-Ara*f* or β-D-Xyl*p*, a di-substitution with α-L-Ara*f* and mono-substitution with oligosaccharides consisting of α-L-Ara*f* and/or β-D-Xyl*p* (Guo, Cui, Wangb, & Young, 2008). Atypical 1,3-linked-β-D-Xyl*p* residues have also been found, suggesting that biosynthesis of AXs in *P. ovata* involves some unusual enzymatic steps (Zeng et al., 2016).

A mechanism for the formation of gels from *P. ovata* AXs has been suggested. It involves the aggregation of unsubstituted blocks in the 1,4-linked-β-D-Xyl*p* backbone to form a gel-like network (Sandhu et al., 1981). However, for highly branched polysaccharides, where unsubstituted blocks are scarce, such mechanism is unlikely. We note that highly branched (comb-like) AXs share structural similarity with other prominent comb-like biopolymers such as animal mucins and proteoglycans. The unique properties of mucins stem from a multitude of possible entangled conformations, and a complex set of polymer relaxation mechanisms (Yakubov, McColl, Bongaerts, & Ramsden, 2009; Yakubov, Papagiannopoulos, Rat, Easton, & Waigh, 2007). It is therefore plausible that highly branched AXs display similar behaviours as mucins, with contributions from entanglements and hydrogen-bond interactions between side-chains during gel formation.

In this work, we aimed to characterise the structure and rheological properties of different AXs extracted from *P. ovata* seed mucilage and elucidate the relationship between side chain structures and gel-forming properties. Furthermore, the distribution of different AXs across the *P. ovata* mucilage thickness has been evaluated. This led to the discovery of a layered structure within the hydrated polysaccharide envelope surrounding the seeds upon exposure to water. Finally, we propose a tentative mechanism for the functions of each layer during mucilage extrusion and discuss their potential biopolymer applications.

## 2. Materials and Methods

### 2.1 Materials

*P. ovata* seeds were provided by Dr Matthew Tucker (University of Adelaide, Australia). Calcofluor white (Fluka) and Direct Red 23 (Aldrich) were used without further purification. All other chemicals were of reagent grade. Endo-1,4-β-xylanase M1 from *Trichoderma viride* and α-L-arabinofuranosidase from *Aspergillus niger* were from Megazyme (Bray, Ireland). All water used in experiments was reverse osmosis treated water (DI water) with resistivity of 18.2 MΩcm (Satorius Stedim).

### 2.2 Mucilage staining and confocal microscope

Confocal images were acquired using an LSM 700 (Zeiss, Germany) inverted confocal laser scanning microscope system, using either a 2.5 x or 10 x objective. The Calcofluor white (CFW) and Direct Red 23 (DR23) fluorescent dyes were used to stain the samples. The dynamic mucilage extrusion video was generated using a time series mode. Five hundred images with the resolution of 512 x 512 pixels were collected over 30 min interval. The pre-stained dry seeds were attached in the centre of a Petri dish using acrylic adhesive (RS Components) and placed on the microscope stage. The experiments started with dry seeds, and after adjustments, 1 mL of DI water was added to the Petri dish to trigger mucilage extrusion.

### 2.3 Mucilage extraction

The mucilage was prepared by sequential extraction procedure based on the work by Guo et al. (2008) with several modifications. Firstly, 20 g of *P. ovata* seeds were dispersed in 800 mL of DI water at 25 ℃ for 4 h under constant stirring. The suspension was then centrifuged at 10,000 g for 30 min. The resulting solution was dialysed at room temperature for 48 h against DI water to obtain cold water (CW) fraction, which was subsequently freeze-dried for further use. The remaining solid phase was dispersed in 400 mL of DI water at 65 ℃ for 4 h under constant stirring. The suspension was then centrifuged at 10,000 g for 30 min. The resulting solution was cooled to 4 ℃ to obtain a gel phase by centrifugation. The gel phase was then washed twice with DI water at 25 ℃, and dispersed in DI water, dialysed against DI water to obtain the hot water (HW) fraction, which was subsequently freeze-dried for further use. The remaining solid phase was dissolved in a 0.2 M KOH solution with 0.01 mg/mL NaBH$_4$ at 25 °C for 4 h, and the solution and residues were separated by centrifugation. The alkaline extract was dialysed at room temperature for 48 h against DI water to obtain the so-called KOH fraction, which was subsequently freeze-dried for further use. The seeds in-between each extraction steps were stained with CFW and DR23 for CSLM analysis.

## 2.4 Monosaccharide composition

Monosaccharide analysis was performed by high-performance anion exchange chromatography coupled with pulsed amperometric detection (HPAEC-PAD). Briefly, 10 mg of samples was extracted by ethanol and chloroform-methanol according to Harholt et al. (2006). The resulting residues were incubated with α-amylase (Sigma-Aldrich, USA) to remove starch, followed by dialysis and hydrolysis in 2 N trifluoroacetic acid for 1 h at 120°C. HPAEC-PAD was performed on an ICS 3000 liquid chromatograph (Dionex) using a CarboPac PA20 anion exchange column (3 × 150 mm; Dionex) as reported in Øbro, Harholt, Scheller, and Orfila (2004).

## 2.5 Glycosidic linkage (methylation) analysis

Uronic acids in a polysaccharide sample (5 mg) were converted to their 6,6-dideuterio neutral sugar counterparts using carbodiimide activation at pH 4.75 followed by sodium borodeuteride ($NaBD_4$) reduction at pH 7.0 (Kim & Carpita, 1992). After dialysis against DI water for 48 h, the carboxyl-reduced sample was collected by freeze-drying. One milligram of the freeze-dried sample (three technical replicates) was then methylated according to Ciucanu and Kerek (1984), with minor modifications. Briefly, the sample was methylated in anhydrous dimethyl sulfoxide (DMSO) by adding 0.3 mL of methyl iodide to the reaction mixture and incubating for 3 h under argon at room temperature with stirring. One mL of dichloromethane (DCM) was subsequently added to the reaction mixture. The methylated polysaccharides dissolved in DCM were extracted by partitioning against DI water (three times) and evaporating the organic phase under a stream of argon, followed by extensive hydrolysis at 100ºC for 6 h in 0.5 mL of 4 M trifluoroacetic acid (TFA) under argon. The hydrolysate was reduced overnight at room temperature in the presence of $NaBD_4$ (5 mg) (under argon) and acetylated with acetic anhydride at 100ºC for 2 hours with stirring. The partially methylated alditol acetates (PMAAs) were recovered by evaporating the solvent under a gentle stream of argon, re-dissolving the sample in DCM, and filtrating the solution through a column filled with anhydrous sodium sulfate powder. The resulting filtrate was transferred to a GC vial and analyzed on a Hewlett Packard 6890/5973 GC-MS equipment fitted with a SP-2380 capillary column (30 m × 0.25 mm i.d., Sigma-Aldrich). Helium was used as carrier gas. For each sample run, the oven temperature was programmed to increase from 165 ºC to 213 ºC at 1 ºC/min, from 213 ºC to 230 ºC at 3 ºC/min, and from 230 ºC to 260 ºC at 10 ºC/min, followed by a plateau at 260 ºC for 10 min (total run time 66.67 min). The mass spectra obtained by electron-impact fragmentation of the different PMAAs were

interpreted by comparing with those of reference derivatives and by referring to literature (Carpita & Shea, 1989).

## 2.6 SEC-MALLS

Three fractions were dissolved (2 mg/mL) overnight under continuous stirring at room temperature in 0.04 M KOH with 60 mmol/L CsCl. The solution was ultrasonicated for 15 min and filtered through a 0.22 μm filter before injection on the liquid chromatography SEC system. The experiment was conducted according to Sullivan et al. (2014) with several modifications. Samples were injected into a Malvern SEC system (Malvern, Germany) using pre-column, Suprema 1000 and Suprema 10,000 (PSS, Germany). The refractive index detector and multi-angle laser light scattering detector (SEC-MALLS 20, Malvern Instruments, UK) were used to monitor the molecular weight distribution. The mobile phase was 0.04 M KOH, the column temperature was 50 °C, and the flow rate was 0.5 mL/min. A series of pullulan standards (Mw from 9.8-1026 kDa, PSS, Germany) was used for the Mark-Houwink method of universal calibration. The pH and ionic strength do not affect hydrodynamic properties of pullulan; accordingly the Mark-Houwink parameters (α=0.67 and k=0.000179) for pullulan in aqueous solvents are based on the data reported in Kasaai (2006). The dn/dc of the CW, HW, and KOH fractions measured by reflectometry were 0.115, 0.135 and 0.121 mL/g, respectively.

## 2.7 Dynamic light scattering

The measurements were performed using a NanoBrook 90Plus Zeta instrument equipped with a 22 mW He-Ne light source ($\lambda$= 657 nm) (Brookhaven, USA). All measurements were performed at the single scattering angle of 90°. To avoid dust contamination, 5 mg/ml stock solutions of samples were prepared in 0.2 M KOH and filtered through low protein binding hydrophilic membrane filters with a pore size of 0.2 μm (Millex®-GS, Millipore). Final solutions were prepared from the stock solutions by diluting with filtered 0.2 M KOH. The solutions were placed in polycarbonate test vials with an i.d. of 8.3 mm. Concentrations examined were in the range of 0.5 – 2 mg/ml in KOH. All measurements were done at 25.0 ± 0.1 °C. The field correlation functions ($g_{(1)}(t,\mathbf{q})$) were all fitted well using a single exponential function, suggesting absence of very broad size distributions. The $R_{DLS}$ were determined using the Stokes-Einstein equation and characteristic relaxation rates extracted from the filed correlation function using the CONTIN method based on the inverse Laplace transform of $g_{(1)}(t,\mathbf{q})$ (Provencher & Štêpánek, 1996).

## 2.8 Determination of intrinsic viscosity and overlap concentration $c^*$

The intrinsic viscosity $[\eta]$ of each fraction in 0.2 M KOH was measured at 25°C by using a Canon-Fenske capillary viscometer (Size 50, 9721-B53). Briefly, the stock concentration for all fractions was kept constant at 2 mg/mL, and viscosity measurements were performed on the diluted samples with different concentration (0.25, 0.5, 0.75, 1.0 mg/mL). The kinetic energy correction was always negligible, since the measurement time ranged from 270 s to 500 s. The $[\eta]$ was obtained from the extrapolation of the specific viscosity ($\eta_{sp} = \frac{\eta - \eta_0}{\eta_0}$, where $\eta_0$ is solvent viscosity) and/or relative viscosity ($\eta_r = \frac{\eta}{\eta_0}$, where $\eta_0$ is solvent viscosity) against concentration to infinite dilution according to the Huggin and Kraemer equation (Huggins, 1942), as follows:

$$\eta_{sp}/c = [\eta] + k[\eta]^2 c \qquad (1)$$

$$\ln(\eta_r)/c = [\eta] + \beta[\eta]^2 c \qquad (2)$$

$\eta_{sp}/c$ is the reduced viscosity, $\ln(\eta_r)/c$ is the inherent viscosity, $c$ is the polymer concentration, and $k$ and $\beta$ are the polymer- and condition-specific constants respectively.

The overlap concentration ($c^*$) of each fraction in 0.2 M KOH was measured at 25 °C using an AR G2 rheometer (TA Instruments, New Castle, DE) equipped with the cone-plate geometry (60 mm of diameter, 2°) (Doyle, Lyons, & Morris, 2009). Briefly, a series of sample solutions (0.375, 0.75, 1.5, 3, 4, 5, 6, 8 mg/mL) was prepared. The zero shear viscosity of these samples were obtained from their flow curve and plotted against concentration.

## 2.9 Small amplitude oscillatory shear rheology measurements

Samples (10 mg/mL) were prepared by dissolving the freeze-dried materials in DI water at 65℃ for 6 hours, and kept for 3 additional h at 85℃ to achieve maximum possible dissolution of samples before the experiments. For the experiments involving enzymatic treatments, samples (8 mg/mL) were dissolved in 0.1 M acetate buffer (NaOAc-HAc, pH 5.6) at 65℃ for 6 hours, and kept for 3 more hours at 85℃ to homogenize or dissolve samples completely. Sixty μL of xylanase M1 (1700U/mL) or 25 μL of α-L-arabinofuranoside (300U/m) were added to 3 mL samples. The same amount of 0.1 M NaOAc-HAc (pH 5.6) buffer was added to the control group.

Small amplitude oscillatory shear (SAOS) measurements were performed using an AR G2 rheometer equipped with the parallel plate geometry (40 mm plate diameter, 0.5 mm gap). Emery paper (P120) was attached to the plate to avoid any slip. The temperature was

9

controlled at the bottom plate using a Peltier unit. All samples were equilibrated at the measuring temperature for 5 min before testing. Solvent traps were used to minimize the effect of solvent evaporation. The dynamic viscoelastic properties were characterized by performing a frequency sweep in the range 10-0.01 Hz at a shear stress of 1 Pa to provide measurements within the linear viscoelastic regime. The temperature ramp for the HW and KOH fractions was performed using SAOS measurements in the temperature ranging from 25 to 85 °C at a frequency of 1 Hz and a shear stress of 1 Pa.

## Results and Discussion

### 3.1 Isolation of the constituent polysaccharides from each mucilage layer

The immersion of *P. ovata* seeds into water triggers mucilage extrusion, which results in the formation of a transparent gel-like capsule (Supplementary Figure 1). Visually, the extrusion process starts within a few seconds after immersion and takes about 20 - 30 min to reach maximum thickness (~1 - 2 mm). By using a mixture of dyes, Calcofluor White (CFW) and Direct Red 23 (DR23), we have identified the presence of at least 3 distinct structural layers during mucilage extrusion (**Fig.** 1A). CFW is considered to bind to β-1,3 and β-1,4 linked polysaccharides (Hughes & McCully, 1975), while DR23 has been shown to preferentially bind to β-1,4 polysaccharides (Anderson, Carroll, Akhmetova, & Somerville, 2010). The outer mucilage layer (L1) is primarily stained with CFW and appears at the onset of polysaccharide extrusion; after a few minutes, the components from this layer diffuse into the surrounding medium. Closer to the seed surface, a gel-like mucilage envelope forms and remains around the seed after mucilage extrusion is complete. Two distinct layers (L2 and L3) are observed under the confocal microscope in a fully hydrated mucilage envelope (**Fig.** 1B). Both are stained with DR 23 and CFW (see Supplementary Figure 2) but there is a distinct intensity gradient between the 'L2' and 'L3' layers. The outer 'L2' domain shows a high intensity of DR23 fluorescence (red), while the inner 'L3' domain yields more CFW fluorescence (green).

In order to isolate the major components from each mucilage layer, sequential extraction was used. Firstly, the readily soluble polysaccharides from the transient 'L1' layer were recovered from the cold water extraction (25°C). Further, polysaccharides from the 'L3' layer of the gel-like envelope were selectively isolated using hot water extraction (65°C). Finally, the polysaccharides from the 'L2' layer of the gel-like envelope were solubilised and

extracted into 0.2M KOH. The extent and selectivity of these extractions were evaluated by imaging the mucilage envelopes in-between extraction steps (see Supplementary Figure 2). As can be seen in Panel D (Supplementary Figure 2) the CFW stained polysaccharides in 'L3' are nearly completely removed after hot water extraction, while after 0.2 M KOH extraction the seed appears to be void of any mucilage layer (Panel E). The components extracted by cold water (25°C), hot water (65°C) and the 0.2 M KOH solution were called CW, HW and KOH fractions, respectively. The yields of these fractions were $4.5 \pm 0.2\%$ (CW), $3.2 \pm 0.1\%$ (HW) and $9.2 \pm 0.4\%$ (KOH) of dry mass of seeds.

Recently, the features of the layered structure in *Arabidopsis* seed mucilage have been further elaborated by Voiniciuc, Yang, Schmidt, Gunl, and Usadel (2015). The pectic polysaccharides are dominant in the *A. thaliana* mucilage, and they are distributed in two layers, namely an outer water-soluble layer and an inner adherent layer (Macquet, Ralet, Kronenberger, Marion-Poll, & North, 2007; William, Lesley, & J.Paul, 2001). The inner adherent layer is further divided into two domains with the innermost layers containing cellulose and $Ca^{2+}$ crosslinked homogalacturonan (Griffiths et al., 2015). Here, we observe a somewhat similar layering structure in the *P. ovata* seed mucilage, except that it consists essentially of AXs. Although there are a number of reports on water-soluble and water-insoluble polysaccharides in seed mucilage, no distinct layered structures have been previously reported in cress seed, chia seed, flax seed or other species (Behrouzian, Razavi, & Karazhiyan, 2014; Capitani, Ixtaina, Nolasco, & Tomás, 2013; Mirhosseini & Amid, 2012; Qian, Cui, Wu, & Goff, 2012; Warrand et al., 2005). Hence, with the exception of *A. thaliana*, the discovered layered structure of *P. ovata* seed mucilage appears to be unique.

### 3.2 Monosaccharide composition and linkage analysis

Monosaccharide composition analysis indicates that xylose and arabinose are the two dominant monosaccharides in all samples (**Table** 1). The ratios of arabinose to xylose of the CW, HW, and KOH fractions are 0.20, 0.30, and 0.33, respectively. Considerable amounts of rhamnose (15.09%) and galacturonic acid (9.65%) residues are detected in the CW fraction. Negligible amounts of glucose are detected in all samples, which points to the occurrence of minute amounts of starch or cellulose.

Glycosidic linkage analysis reveals a highly branched structure and a distinct linkage composition of the AXs from *Plantago* mucilage, compared to other AXs from cereals, e.g., wheat or barley. Recently, highly branched AXs were identified in New Zealand flax

11

(Centanni et al., 2017), yet these AXs contain less 1,3-linked xylose residues and no 1,3-linked arabinose residues compared to AXs from *P. ovata* mucilage. The ratio of terminal units to branching points in our samples is approximately one (CW=1.19, HW=1.22, and KOH=1.16), which is consistent with the expectation that the number of branching point units (1,2,4-Xyl*p*, 1,3,4-Xyl*p*, and 1,2,3,4-Xyl*p* ) should approximately equal the number of non-reducing terminal units (t-Rha*p*, t-GlcA*p*, t-GalA*p*, t-Gal*p*, t-Ara*f* and t-Xyl*p*) in polysaccharides. At least 30 - 45% of sugar residues in total are located in side chains, since the non-reducing terminal units of CW, HW and KOH fractions represent ~ 30 - 45% of the total monosaccharides, which indicates that the polysaccharides are combs (**Table** 2). More than 50% of these terminal units are t-Xyl*p*, which is quite different to AX from cereals. Almost all the non-reducing terminal units of wheat or barley AXs reported in the literature are t-Ara*f*, so the degree of branching in these polymer chains can be roughly estimated based on the ratio of arabinose to xylose (Cui, 2000). Another unique characteristic of AX from *Plantago* mucilage is the large amount of 1,3-linked Xyl*p* in its structure. It is still unknown whether this 1,3-Xyl*p* is on the backbone or side chains. According to the study of Fischer et al. (2004), the β-1,3-linked D-Xyl*p* is assigned to the side chain because the NMR data support the occurrence of oligosaccharide L-Ara*f*-α-(1→3)-D-Xyl*p*-β-(1→3)-L-Ara*f* after partial acid hydrolysis. A number of researchers have proposed structural models for AXs from *Plantago* or psyllium husk based on this assumption (Guo et al., 2008; Van Craeyveld, Delcour, & Courtin, 2009). However, it is believed that →4)-D-Xyl*p*-β-(1→3)-D-Xyl*p*-β-(1→ is also possible to alternatively occur in the main chain (Sandhu et al., 1981). Although the fine-level structures of these polysaccharides are not clear, it is believed that their unique properties, e.g. resistance to fermentation in the human large intestine, has a close relation to their atypical linkages and side chain structures (Marlett & Fischer, 2002). For example, the complex AX from New Zealand flax has been shown to display limited fermentability by the gut *B. cellulosilyticus*, due to limited ability of the bacterium to cleave off the side chains from the substrate (Centanni et al., 2017).

The three fractions isolated from *Plantago* mucilage have similar linkage composition, but the CW fraction has more complex linkages and large amounts of 1,2-linked Rha*p* and 1,4-linked GalA*p* residues. The abundance (20%) of negatively charged GalA*p* residues in the CW fraction is a plausible explanation for its high solubility in water at 25°C. Additionally,

12

the presence of Rha*p* indicates that AX aside, the CW fraction contains rhamnogalacturonic pectin that is essentially linear (See a note to Supplementary Figure 8).

By contrast, the HW and KOH fractions show markedly different solubility in water and affinity to CFW and DR23 staining, yet both of them have strikingly similar monosaccharide and linkage compositions. The similarity of chemical composition of HW and KOH fractions are further supported by comparing their 1D-NMR spectra (see Supplementary Figure 3), which are virtually identical. Several small peaks at around 2.0-2.2 ppm were identified in the HW fraction but were absent in the KOH fraction, which may be associated with some differences in the degree of O-acetylation (Sims & Newman, 2006).

### 3.3 HPSEC-MALLS and molecular shape

According to the results of the HPSEC-MALLS experiments (Supplementary Figure 4), all three fractions have low polydispersity index ($\leq 1.5$) and high recovery rate ($>80\%$). This result reveals that samples dissolve well in the mobile phase. In addition, the offset in the peak position between the DRI and MALLS detector signals has also been found very small (see Supplementary Figure 4), further indicating that the aggregation effect is negligible in all fractions. The weight average molecular weights (Mw) are very similar across all three fractions, ranging from 950 to 1100 kDa. Nonetheless, as listed in **Table** 3, the molecular shape of these fractions appears to be rather different since they have distinct intrinsic viscosity ($[\eta]$), overlap concertation ($c^*$), radii of gyration ($R_g$) and hydrodynamic radii.

The $[\eta]$ values range from 3.1 dL/g for the CW fraction to 7.4 dL/g for the KOH fraction. The hydrodynamic radius is calculated from $[\eta]$ using the Einstein equation: $R_{[\eta]} = \sqrt[3]{\dfrac{3M_w[\eta]}{10\pi N_A}}$, where $N_A$ is the Avogadro constant (Einstein, 1906). For the HW and KOH fractions, the calculated $R_{[\eta]}$ values are nearly identical to the hydrodynamic radius obtained from the SEC-MALLS ($R_h$) experiments and DLS ($R_{DLS}$). This consistency enables us to assign the $R_h$ of polysaccharides from *P. ovata* seed mucilage, which is only slightly smaller than Guo's DLS measurement (50 - 70 nm) of *Plantago* mucilage polysaccharides in 0.5M NaOH (Guo et al., 2008).

Another key molecular parameter is $R_g$, which is evaluated using batch processed MALLS data. The three fractions have similar $R_g$, in the range 40-50 nm. The large molecular weight but small molecular volume and size (small $[\eta]$, $R_h$ and $R_g$) indicate that the polysaccharides from *P. ovata* seed mucilage adopt a rather compact conformation in alkaline solution. This is

illustrated by calculating the structural parameter ($\rho=R_g/R_h$). The $\rho$ of mucilage polysaccharides in this study spans from 0.89 to 1.21, which reveals their tendency to adopt compact coil conformations that can be classified as being intermediate between a fully compact sphere ($\approx$0.77) and a completely random coil ($\approx$1.78) (Schweins & Huber, 2001). These conformations may be attributed to some level of self-aggregation due to the presence of intra-molecular hydrogen bonds. In addition, the hyper-branched nature of the polysaccharides may also contribute to the observed compact structures. Tao, Zhang, Yan, and Wu (2007) reported that water-insoluble hyper-branched β-glucans from fungal species occur as compact chain conformations with a sphere-like structure in DMSO solution. Although all three *Plantago* fractions adopt compact conformations, the values of $\rho$ are different among three fractions. In particular, we note a marked difference between the HW and KOH fractions that compositionally are very similar, yet the polysaccharides in the HW fraction adopt a more open conformation ($\rho = 1.21$) compared to that of the KOH fraction ($\rho = 0.93$). This evidence emphasizes the distinctiveness of the conformational structures in these fractions despite similarities in monosaccharide and linkage compositions. The difference in *O*-acetylation, albeit minimal, may still contribute to these differences.

## 3.4 Rheological properties

The mechanical spectrum of the three fractions at a concentration of 1% w/v in water at 25 °C is shown in Figure 2. The CW fraction displays a viscoelastic fluid response since its loss modulus G'' is higher than the storage modulus G' (tanδ > 1, **Fig.** 2A and D). In contrast, the HW and KOH fractions display gel-like behaviours since G' > G'' across the frequency range (tan δ < 1), as shown in **Fig.** 2B, C and D. The moduli and tanδ for the KOH fraction are relatively independent of frequency and tanδ ~ 0.1, which indicates it is classifiable as a gel. In contrast, higher values of tanδ are observed for the HW 'gel' whilst its moduli are strongly dependent on frequency ($G' \sim \omega^{0.4}$), which indicates it is more viscous and liquid-like than the KOH fraction (**Fig.** 2D).

Another difference between the HW and KOH gels is their sensitivity to temperature. The HW 'gel' melts upon increase in temperature to 41 ± 2°C, whereas the KOH gel largely retains its mechanical properties even when heated to temperatures as high as 85°C (**Fig.** 3). We note that no hysteresis effects in mechanical spectra are observed upon heating up and cooling down for both the HW and KOH fractions.

### 3.5 Relationship between structure and rheological properties of the gel-forming AX fractions of *P. ovata* mucilage

The aim of the work presented in this section was to rationalise the distinct rheological behaviours of two neutral gel-forming fractions with nearly identical monosaccharide and linkage compositions. Commonly, the rheological properties of polysaccharides are determined by their polymer structure (Cui, 2005). However, for mucilage AXs, additional factors must be considered, such as ferulic-acid mediated cross-links and the presence of admixtures.

Following these basic concepts, we corroborate the mechanism of gelation in both gel-forming fractions by narrowing them down to three possible scenarios. In the first scenario we explore the possibility of ferulic acid links, which may be present at different concentrations in both fractions. The second scenario explores a possibility of colloidal cellulose fibril particles being present within one of the gels. The third scenario explores the effect of side chains and possible involvement of side-chain hydrogen-bond interactions to promote formation of a physical gel.

According to data in the literature, the presence of ferulic acid, which forms cross-links between neighbouring AX chains, is the main reason for gel formation of AXs from wheat or barley (Carvajal-Millan et al., 2005; Niño-Medina et al., 2010). Recently, ferulic acid has also been found in polysaccharides from *P. assissa* seeds, which could form cross-links among molecules to enhance gel strength in the presence of $Ca^{2+}$ (Yin et al., 2012). However, our results suggest that the presence of ferulic acid links is unlikely to be the key driver of gel formation of mucilage polysaccharides from *P. ovata*. Firstly, our data point to the absence of temperature hysteresis in gels formed from the HW and KOH fractions (**Fig.** 3), which strongly indicates that both form a physical gel rather than a chemically cross-linked gel. The term 'physical gel' refers to chain association and particle aggregation involving non-covalent cross-links such as hydrophobic, electrostatic and hydrogen bonding interactions (Stokes, 2012). In contrast to 'chemical gels', thermos-reversibility is a signature of a 'physical gel' system (Ross‐Murphy, 1995). Another compelling evidence to support the 'physical gel' hypothesis is that 8 M GuHCl, known as a hydrogen bond disruptor, dissolves the gel formed by both fractions, which indicates that hydrogen bonding is key to the formation of a gel network (see Supplementary Figure 5). Finally, upon neutralising both the HW and KOH fractions, the exact same gels re-form after ferulic acid residues have been hydrolysed in 2 M NaOH at 25°C. In order to further probe the possible effect of ferulic acid,

we have performed an analytical evaluation of the ferulic acid content of the fractions. Here, the expectation is that the gel strength would correlate with ferulic acid content. The analysis shows that the softer gel (HW fraction) contains 0.39±0.03 mg/g of ferulic acid, while the stronger gel (KOH fraction) is characterized by significantly lower amounts of ferulic acid (0.14±0.02 mg/g). Taking all evidence together enables us to exclude the ferulic acid links as a plausible structure that (i) underpins the gelation mechanism in both gel-forming fractions, and (ii) explains the differences between their mechanical properties.

In *Arabidopsis* mucilage, cellulose fibres are found to act as a 'skeleton', which anchors pectic polysaccharides to the seed coat (Macquet et al., 2007). Theoretically, it could be possible that nano-scale cellulose fibres are present in the extracted gel-forming fractions as a dispersed colloid. In this scenario, we would surmise that even at very small concentrations these fibrous particles would affect the mechanical spectra of the gels. We indeed detected very small amounts of glucose in both gel-forming fractions, albeit with no significant difference between the two fractions (as shown in **Table** 1&2, Glc < 0.6%, 1,4-Glc$p$ < 0.3%). In order to visualize and differentiate cellulose content in both fractions, atomic force microscopy was utilised to observe the residues after the treatment of the extracted mucilage fraction with the Updegraff reagent to remove all non-crystalline polysaccharides (Updegraff, 1969). In both fractions one can observe some filament-like structures that can be attributed to the residual colloid-sized cellulose-fibres (Supplementary Figure 6). The basic image analysis and particle count has not revealed a statistically significant difference between the two fractions, suggesting that even though colloidal cellulose is present in *P. ovata* mucilage, it is unlikely to be responsible for the difference in the gelling behaviour of the HW and KOH fractions. That said, the presence of cellulose may still affect the properties of mucilage around the seed (i.e. prior to extraction), which should stimulate future research directed at elucidating rheological properties of mucilage layers *in situ*. Finally, the HW and KOH fractions can maintain their gel structure after cellulase treatment (tan δ<1, see Supplementary Figure 7), which further supports the conclusion that colloidal cellulose fibres are not the key structural element responsible for the distinct gel properties of the HW and KOH fractions.

We also considered the possibility that differences in *O*-acetylation between the HW and KOH fractions may be responsible for the observed rheological differences. We hypothesise that the polysaccharides in the HW fraction have more acetylated groups than their counterpart from the KOH fraction because the KOH fraction was obtained using a base. To

test this hypothesis, the HW fraction was treated with KOH solutions that are known to partially hydrolyse acetylated groups on xylan backbones. Using both 0.2 M KOH (same concentration as used in extracting KOH fraction) and 2M KOH solutions, we found that none of these two KOH treatments induced any change in the rheological properties of the HW fraction. Therefore, we concluded that the difference in acetylation is not the major reason for the observed rheological differences between the HW and KOH fractions.

The formation of a physical gel indicates the transience of the links between polysaccharide chains, which we hypothesise is associated with hydrogen bonding between the side-chains or side-chains and the backbones. Although this mechanism is plausible to explain gelation, it is challenging to demonstrate clearly the fine-level details of the molecular architecture of the polysaccharides in the HW and KOH fractions that would underpin their distinct mechanical properties.

The difference in structure between the HW and KOH fractions can be clearly inferred from the SEC-MALLS and intrinsic viscosity data (**Table** 3) that indicate different molecular architectures of constituent AXs. In order to further test this hypothesis, xylanase M1 and α-L-arabinofuranosidase (*Aspergillus niger*) was used to degrade the HW and KOH fraction gels. M1 (GH family 11) selectively cleaves the internal β-1,4 linkages between unsubstituted D-Xyl*p* residues within the backbone and is widely used to hydrolyse the backbone of AXs (**Fig.** 4 A) (Biely, Vršanská, Tenkanen, & Kluepfel, 1997; Collins, Gerday, & Feller, 2005). The α-L-arabinofuranosidase from *A. niger* (GH family 51) can act on both α-1,2- and/or α-1,3- and/or α-1,5-linked L-Ara*f* residues within side chains, and it is generally used to de-branch AXs (Saha, 2000) (**Fig.** 4 A). As shown in **Fig.** 4, both G' and $\tan\delta$ remain unaffected after the xylanase M1 treatment, which indicates that the HW and KOH fractions maintain their gel structure after enzymatic treatment. By contrast, α-L-arabinofuranosidase treatment completely abates gelling of the HW fraction; G' significantly decreases from 20 Pa to < 0.02 Pa and the corresponding $\tan\delta$ becomes higher than 1. The effect of α-L-arabinofuranosidase hydrolysis on the KOH fraction is found to be marginal compared to the HW fraction. The values of $\tan\delta$ only show small changes with and without enzyme treatment (**Fig.** 4), while G' exhibits only a slight change, indicating that cleavage does occur but without much effect on the gel network. Further monosaccharide analysis confirms that appreciable amounts of arabinose are released from the KOH fraction upon α-L-arabinofuranosidase hydrolysis (supplementary material). According to these results, we conclude that gels from the HW and KOH fractions show different susceptibility to

hydrolytic enzymes, especially α-L-arabinofuranosidase, which demonstrates differences in their structure on the level of fine details.

The activity of GH11 xylanases are easily hindered by the presence of side groups. Thus, these enzymes can only act on β-1,4 linkages present between two unsubstituted xylose residues (Paës, Berrin, & Beaugrand, 2012). The highly branched structure of both gel-forming fractions probably explains the lack of significant enzymatic hydrolysis. The GH51 α-L-arabinofuranosidase (*A. niger*) is found to preferentially hydrolyze Ara*f* residues on single substituted Xyl*p* residues and slowly act on Ara*f* of di-substituted Xyl*p* (Köhnke, Östlund, & Brelid, 2011). Therefore, the terminal Ara*f* on single substituted Xyl*p* residues must play an important role on gel formation in the HW fraction, while for the KOH fraction the gelation have to be associated with the hydrogen bonding involving terminal D-Xyl*p* or 1-3 linked D-Xyl*p* within side chains. The latter hypothesis has been further tested in experiments conducted using other enzymes and enzyme combinations (β-D-xylosidase, xylanase M6 from GH family 11, and arabinofuranosidase M2 from GH family 43), which all showed negligible effects on the gel properties of the KOH fraction.  In an attempt to estimate the upper limit of hydrolytic resistance of the KOH fraction, we treated this fraction with mild trifluoroacetic acid (TFA) (100 mM, 70 °C, 1h), which is known to preferentially hydrolyse side chains.  The TFA treatment resulted in a complete loss of the gel-forming capacity of the KOH fraction. Although TFA treatment is unspecific, and breakage of backbone cannot be entirely excluded, we suggest that this test provides some useful evidence for the role of side-chains as a leading mechanism of gel formation in *P. ovata* AX mucilage.  We hypothesise that a unique distribution pattern of side chains or atypical linkages in the main chain (e.g., presence of β-1,3-linked D-Xyl*p*) may be responsible for the differences in the rheological behaviour between the KOH- and HW-extractable *P. ovata* AXs.

## Concluding remarks

We have discovered that, in contact with water, *P. ovata* seeds secrete three fluid mucilage layers, which contain multiple comb-like AX polysaccharides of similar composition and molecular weight. The CW fraction from the outermost layer (L1) is rich in galacturonic acid residues, which makes it highly soluble in water at 25°C. In contrast, the neutral fractions (HW and KOH fractions) from the inner layers of mucilage envelope form different gels in water at 25°C. By using chaotropic solvents (8M guanidium chloride) and enzymatic

hydrolysis, we demonstrated that the hydrogen bonding involving side chains is a key mechanism of gel formation in both fractions, and the subtle changes in arabinose/xylose side chain structure are likely to be the reason for the observed rheological differences.

In considering mechanisms occurring during seed hydration, the results suggest that the high affinity for water of the cold water-soluble AX fraction is a key driver for the mucilage to 'erupt' from seed upon contact with water, whereby AXs rapidly solubilise to form a viscoelastic liquid outer layer (see Supplementary video). The AXs extruded next undergo gelation in the water, which slows their movement out of the seed; the gels provide a protective viscoelastic shell around the seed and allow water molecules to remain in close proximity. The differences in fine structure of these AXs may enable formation of functional mucilage gels and a 'water reservoir' around seeds under variable environmental conditions that include temperature and salinity. It is anticipated that future studies will elucidate these hypotheses further and substantiate the role of polysaccharides in mucilage function and responsiveness.

In addition to uncovering the mechanistic role of mucilage polysaccharides in seed physiology, which is valuable from an agricultural perspective, the unique observation of forming multilayered coating using relatively similar polymer molecules may inspire innovative ideas in biomimetic engineering. For example, rationally engineered layered structures have potential use as functional coatings of encapsulates for targeted delivery (e.g., microgels) to specific locations in the gastrointestinal tract or other locations in the human body, and in creating low friction surfaces in aqueous environments; both of these have strategic value to a range of food, pharmaceutical and biomedical applications.

## Acknowledgements

# References

Anderson, C. T., Carroll, A., Akhmetova, L., & Somerville, C. (2010). Real-Time Imaging of Cellulose Reorientation during Cell Wall Expansion in Arabidopsis Roots. *Plant Physiology,* 152(2), 787-796.

Behrouzian, F., Razavi, S. M. A., & Karazhiyan, H. (2014). Intrinsic viscosity of cress (Lepidium sativum) seed gum: Effect of salts and sugars. *Food Hydrocolloids,* 35, 100-105.

Biely, P., Vršanská, M., Tenkanen, M., & Kluepfel, D. (1997). Endo-β-1, 4-xylanase families: differences in catalytic properties. *Journal of biotechnology,* 57(1), 151-166.

Broekaert, W. F., Courtin, C. M., Verbeke, K., Van de Wiele, T., Verstraete, W., & Delcour, J. A. (2011). Prebiotic and other health-related effects of cereal-derived arabinoxylans, arabinoxylan-oligosaccharides, and xylooligosaccharides. *Critical reviews in food science and nutrition,* 51(2), 178-194.

Capitani, M. I., Ixtaina, V. Y., Nolasco, S. M., & Tomás, M. C. (2013). Microstructure, chemical composition and mucilage exudation of chia (Salvia hispanica L.) nutlets from Argentina. *Journal of the Science of Food and Agriculture,* 93(15), 3856-3862.

Carpita, N. C., & Shea, E. M. (1989). Linkage structure of carbohydrates by gas chromatography-mass spectrometry (GC-MS) of partially methylated alditol acetates. *Analysis of Carbohydrates by GLC and MS*, 157-216.

Carvajal-Millan, E., Landillon, V., Morel, M.-H., Rouau, X., Doublier, J.-L., & Micard, V. (2005). Arabinoxylan gels: Impact of the feruloylation degree on their structure and properties. *Biomacromolecules,* 6(1), 309-317.

Centanni, M., Hutchison, J. C., Carnachan, S. M., Daines, A. M., Kelly, W. J., Tannock, G. W., & Sims, I. M. (2017). Differential growth of bowel commensal Bacteroides species on plant xylans of differing structural complexity. *Carbohydr Polym,* 157, 1374-1382.

Ciucanu, I., & Kerek, F. (1984). A simple and rapid method for the permethylation of carbohydrates. *Carbohydrate Research,* 131(2), 209-217.

Collins, T., Gerday, C., & Feller, G. (2005). Xylanases, xylanase families and extremophilic xylanases. *FEMS microbiology reviews,* 29(1), 3-23.

Cui, S. W. (2000). *Polysaccharide gums from agricultural products: Processing, structures and functionality*: CRC Press.

Cui, S. W. (2005). *Food carbohydrates: chemistry, physical properties, and applications*: CRC Press.

Doyle, J. P., Lyons, G., & Morris, E. R. (2009). New proposals on "hyperentanglement" of galactomannans: Solution viscosity of fenugreek gum under neutral and alkaline conditions. *Food Hydrocolloids,* 23(6), 1501-1510.

Edwards, S., Chaplin, M. F., Blackwood, A. D., & Dettmar, P. W. (2003). Primary structure of arabinoxylans of ispaghula husk and wheat bran. *Proc Nutr Soc,* 62(1), 217-222.

Einstein, A. (1906). A new determination of molecular dimensions. *Ann. Phys,* 19(2), 289-306.

Fischer, M. H., Yu, N. X., Gray, G. R., Ralph, J., Anderson, L., & Marlett, J. A. (2004). The gel-forming polysaccharide of psyllium husk (Plantago ovata Forsk). *Carbohydrate Research,* 339(11), 2009-2017.

Griffiths, J. S., Sola, K., Kushwaha, R., Lam, P., Tateno, M., Young, R., Haughn, G. W. (2015). Unidirectional movement of cellulose synthase complexes in Arabidopsis seed coat

epidermal cells deposit cellulose involved in mucilage extrusion, adherence, and ray formation. *Plant Physiology,* 168(2), 502-520.

Guo, Q., Cui, S. W., Wangb, Q., & Young, J. C. (2008). Fractionation and physicochemical characterization of psyllium gum. *Carbohydrate Polymers,* 73(1), 35-43.

Harholt, J., Jensen, J. K., Sørensen, S. O., Orfila, C., Pauly, M., & Scheller, H. V. (2006). ARABINAN DEFICIENT 1 is a putative arabinosyltransferase involved in biosynthesis of pectic arabinan in Arabidopsis. *Plant Physiology,* 140(1), 49-58.

Höije, A., Sternemalm, E., Heikkinen, S., Tenkanen, M., & Gatenholm, P. (2008). Material properties of films from enzymatically tailored arabinoxylans. *Biomacromolecules,* 9(7), 2042-2047.

Huang, Z., Boubriak, I., Osborne, D. J., Dong, M., & Gutterman, Y. (2008). Possible role of pectin-containing mucilage and dew in repairing embryo DNA of seeds adapted to desert conditions. *Annals of Botany,* 101(2), 277-283.

Huggins, M. L. (1942). The viscosity of dilute solutions of long-chain molecules. IV. Dependence on concentration. *Journal of the American Chemical Society,* 64(11), 2716-2718.

Hughes, J., & McCully, M. E. (1975). The use of an optical brightener in the study of plant structure. *Stain technology,* 50(5), 319-329.

Ishii, T. (1997). Structure and functions of feruloylated polysaccharides. *Plant Science,* 127(2), 111-127.

Izydorczyk, & Dexter, J. (2008). Barley β-glucans and arabinoxylans: molecular structure, physicochemical properties, and uses in food products–a review. *Food Research International,* 41(9), 850-868.

Izydorczyk, M. S., & Biliaderis, C. G. (1995). Cereal arabinoxylans: advances in structure and physicochemical properties. *Carbohydrate Polymers,* 28(1), 33-48.

Kasaai, M. R. (2006). Intrinsic viscosity–molecular weight relationship and hydrodynamic volume for pullulan. *Journal of applied polymer science,* 100(6), 4325-4332.

Kennedy, J. F., Sandhu, J. S., & Southgate, D. A. T. (1979). Structural Data for the Carbohydrate of Ispaghula Husk Ex Plantago-Ovata Forsk. *Carbohydrate Research,* 75(Oct), 265-274.

Kim, J.-B., & Carpita, N. C. (1992). Changes in esterification of the uronic acid groups of cell wall polysaccharides during elongation of maize coleoptiles. *Plant Physiology,* 98(2), 646-653.

Köhnke, T., Östlund, Å., & Brelid, H. (2011). Adsorption of arabinoxylan on cellulosic surfaces: influence of degree of substitution and substitution pattern on adsorption characteristics. *Biomacromolecules,* 12(7), 2633-2641.

Kreitschitz, A., Kovalev, A., & Gorb, S. N. (2015). Slipping vs sticking: Water-dependent adhesive and frictional properties of Linum usitatissimum L. seed mucilaginous envelope and its biological significance. *Acta Biomaterialia,* 17, 152-159.

Macquet, A., Ralet, M. C., Kronenberger, J., Marion-Poll, A., & North, H. M. (2007). In situ, chemical and macromolecular study of the composition of Arabidopsis thaliana seed coat mucilage. *Plant and Cell Physiology,* 48(7), 984-999.

Marlett, J. A., & Fischer, M. H. (2002). A poorly fermented gel from psyllium seed husk increases excreta moisture and bile acid excretion in rats. *The Journal of nutrition,* 132(9), 2638-2643.

Mirhosseini, H., & Amid, B. T. (2012). A review study on chemical composition and molecular structure of newly plant gum exudates and seed gums. *Food Research International,* 46(1), 387-398.

Niño-Medina, G., Carvajal-Millán, E., Lizardi, J., Rascon-Chu, A., Marquez-Escalante, J. A., Gardea, A., . . . Guerrero, V. (2009). Maize processing waste water arabinoxylans: Gelling capability and cross-linking content. *Food Chemistry,* 115(4), 1286-1290.

Niño-Medina, G., Carvajal-Millán, E., Rascon-Chu, A., Marquez-Escalante, J. A., Guerrero, V., & Salas-Muñoz, E. (2010). Feruloylated arabinoxylans and arabinoxylan gels: structure, sources and applications. *Phytochemistry Reviews,* 9(1), 111-120.

Øbro, J., Harholt, J., Scheller, H. V., & Orfila, C. (2004). Rhamnogalacturonan I in Solanum tuberosum tubers contains complex arabinogalactan structures. *Phytochemistry,* 65(10), 1429-1438.

Paës, G., Berrin, J.-G., & Beaugrand, J. (2012). GH11 xylanases: structure/function/properties relationships and applications. *Biotechnology advances,* 30(3), 564-592.

Provencher, S. W., & Štêpánek, P. (1996). Global analysis of dynamic light scattering autocorrelation functions. *Particle & particle systems characterization,* 13(5), 291-294.

Qian, K. Y., Cui, S. W., Wu, Y., & Goff, H. D. (2012). Flaxseed gum from flaxseed hulls: Extraction, fractionation, and characterization. *Food Hydrocolloids,* 28(2), 275-283.

Ross‐Murphy, S. B. (1995). Structure–property relationships in food biopolymer gels and solutions. *Journal of Rheology (1978-present),* 39(6), 1451-1463.

Saha, B. C. (2000). α-L-Arabinofuranosidases: biochemistry, molecular biology and application in biotechnology. *Biotechnology advances,* 18(5), 403-423.

Sandhu, J. S., Hudson, G. J., & Kennedy, J. F. (1981). The Gel Nature and Structure of the Carbohydrate of Ispaghula Husk Ex-Plantago-Ovata Forsk. *Carbohydrate Research,* 93(2), 247-259.

Schweins, R., & Huber, K. (2001). Collapse of sodium polyacrylate chains in calcium salt solutions. *The European Physical Journal E,* 5(1), 117-126.

Sims, I. M., & Newman, R. H. (2006). Structural studies of acidic xylans exuded from leaves of the monocotyledonous plants Phormium tenax and Phormium cookianum. *Carbohydrate Polymers,* 63(3), 379-384.

Stokes, J. R. (2012). Food biopolymer gels, microgel and nanogel structures, formation and rheology.

Sullivan, M. A., Powell, P. O., Witt, T., Vilaplana, F., Roura, E., & Gilbert, R. G. (2014). Improving size-exclusion chromatography separation for glycogen. *Journal of Chromatography A,* 1332, 21-29.

Sun, X.-F., Wang, H.-h., Jing, Z.-x., & Mohanathas, R. (2013). Hemicellulose-based pH-sensitive and biodegradable hydrogel for controlled drug delivery. *Carbohydrate Polymers,* 92(2), 1357-1366.

Tao, Y. Z., Zhang, L., Yan, F., & Wu, X. J. (2007). Chain conformation of water-insoluble hyperbranched polysaccharide from fungus. *Biomacromolecules,* 8(7), 2321-2328.

Updegraff, D. M. (1969). Semimicro determination of cellulose inbiological materials. *Analytical biochemistry,* 32(3), 420-424.

Van Craeyveld, V., Delcour, J. A., & Courtin, C. M. (2009). Extractability and chemical and enzymic degradation of psyllium (Plantago ovata Forsk) seed husk arabinoxylans. *Food chemistry,* 112(4), 812-819.

Voiniciuc, C., Yang, B., Schmidt, M. H. W., Gunl, M., & Usadel, B. (2015). Starting to Gel: How Arabidopsis Seed Coat Epidermal Cells Produce Specialized Secondary Cell Walls. *International Journal of Molecular Sciences,* 16(2), 3452-3473.

Vorwerk, S., Somerville, S., & Somerville, C. (2004). The role of plant cell wall polysaccharide composition in disease resistance. *Trends in plant science,* 9(4), 203-209.

Warrand, J., Michaud, P., Picton, L., Muller, G., Courtois, B., Ralainirina, R., & Courtois, J. (2005). Contributions of intermolecular interactions between constitutive arabinoxylans to the flaxseeds mucilage properties. *Biomacromolecules,* 6(4), 1871-1876.

William, G. T. W., Lesley, M., & J.Paul, K. (2001). In-suit analysis of pectic polysaccharide in seed mucilage and at the root surface of *Arabidopsis thaliana*. *Planta,* 213, 37-44.

Yadav, M. P., Hicks, K. B., Johnston, D. B., Hotchkiss, A. T., Chau, H. K., & Hanah, K. (2016). Production of bio-based fiber gums from the waste streams resulting from the commercial processing of corn bran and oat hulls. *Food Hydrocolloids,* 53, 125-133.

Yakubov, G. E., McColl, J., Bongaerts, J. H., & Ramsden, J. J. (2009). Viscous boundary lubrication of hydrophobic surfaces by mucin. *Langmuir,* 25(4), 2313-2321.

Yakubov, G. E., Papagiannopoulos, A., Rat, E., Easton, R. L., & Waigh, T. A. (2007). Molecular structure and rheological properties of short-side-chain heavily glycosylated porcine stomach mucin. *Biomacromolecules,* 8(11), 3467-3477.

Yang, X. J., Baskin, J. M., Baskin, C. C., & Huang, Z. Y. (2012). More than just a coating: Ecological importance, taxonomic occurrence and phylogenetic relationships of seed coat mucilage. *Perspectives in Plant Ecology Evolution and Systematics,* 14(6), 434-442.

Yin, J. Y., Nie, S. P., Li, J., Li, C., Cui, S. W., & Xie, M. Y. (2012). Mechanism of Interactions between Calcium and Viscous Polysaccharide from the Seeds of Plantago asiatica L. *Journal of Agricultural and Food Chemistry,* 60(32), 7981-7987.

Zeng, W., Lampugnani, E. R., Picard, K. L., Song, L., Wu, A., Farion, I. M., Bacic, A. (2016). Asparagus IRX9, IRX10 and IRX14A are essential for xylan biosynthesis in the Golgi apparatus of Asparagus. *Plant physiology*, pp. 01919.02015.
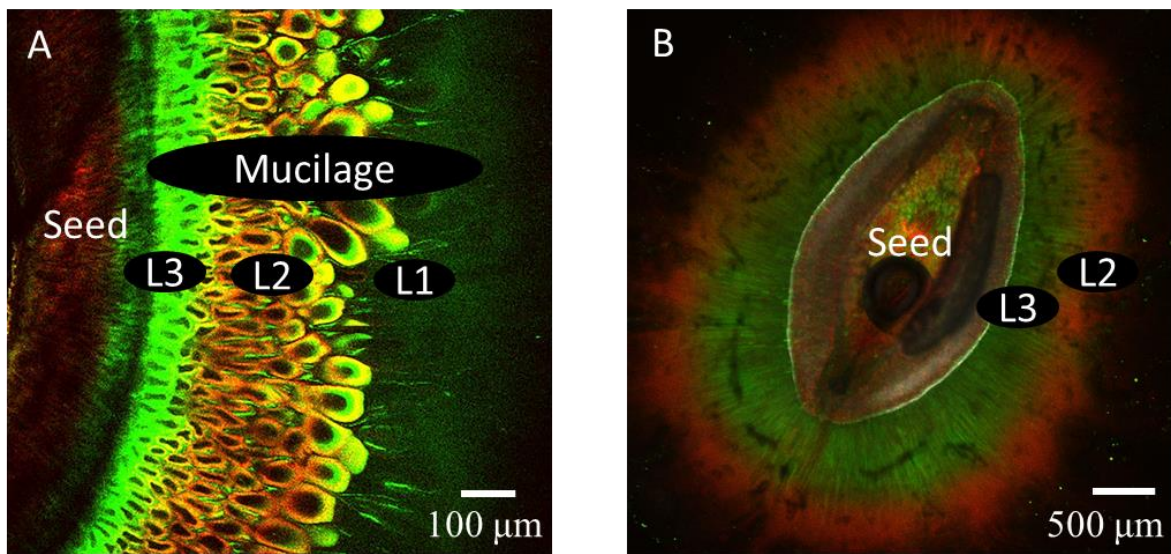
**Figure 1** Images of *Plantago ovata* mucilage staining with Calcofluor white (CFW Green) and Direct Red 23 (DR23 Red) under LSM 700 confocal microscopy (**A**. mucilage at the onset of extrusion, **B.** mucilage at the end of extrusion)
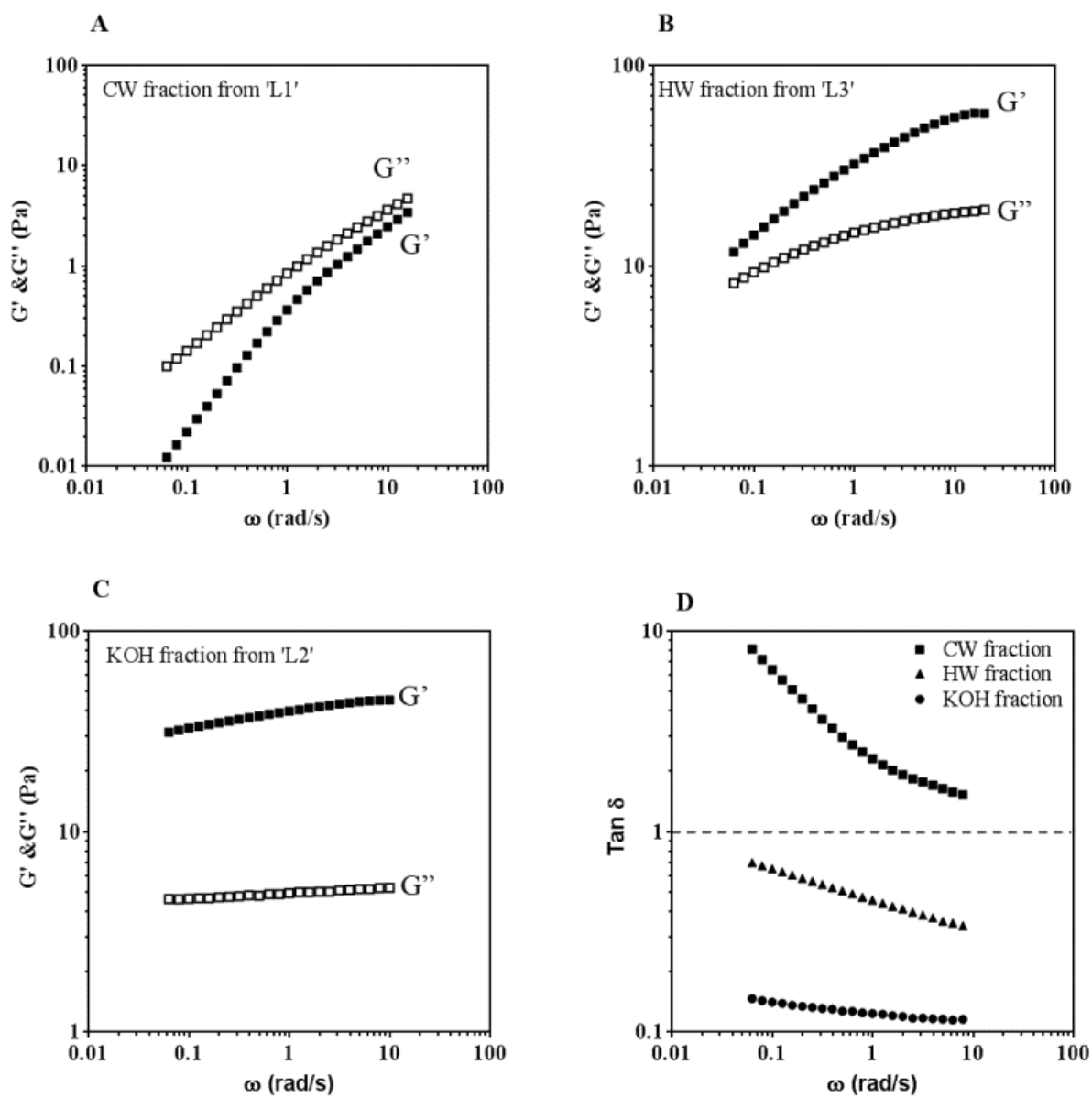
**Figure 2** Frequency sweep of 1 % (w/v) sample in water. (**A.** CW fraction; **B** HW fraction; **C.** KOH fraction; **D.** tan δ against frequency)
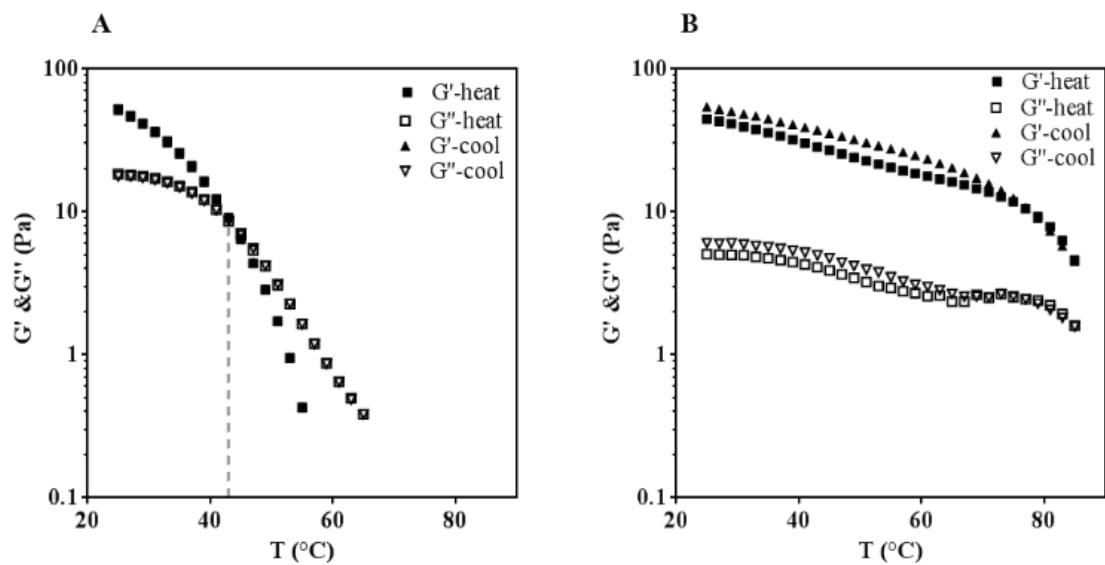
**Figure 3** Temperature sweep of 1 % (w/v) sample in water (**A.** HW fraction; **B.** KOH fraction; G'-heat & G"-heat means increasing temperature from 25 to 85 °C; G'-cool & G"-cool means decreasing temperature from 85 to 25 °C)
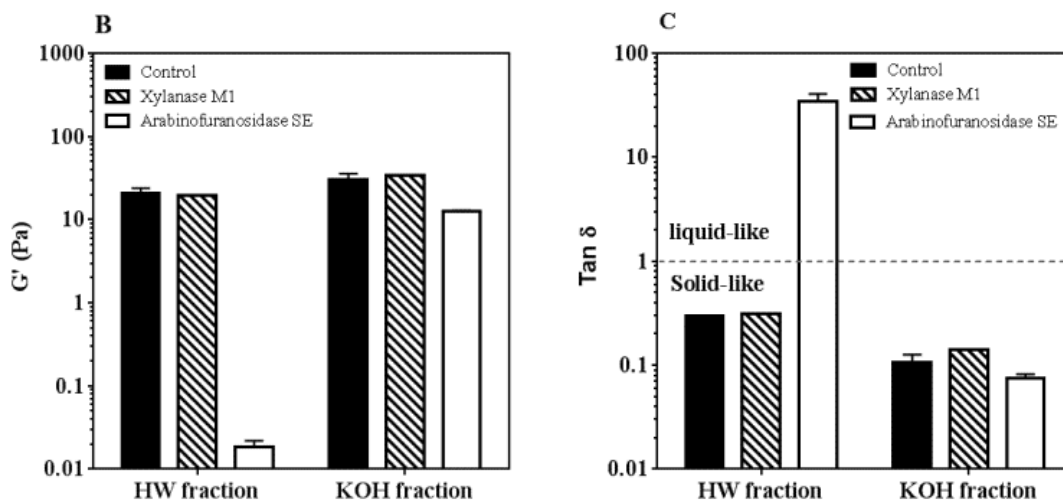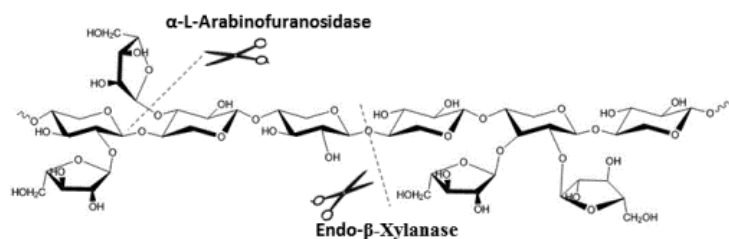
**Figure 4** The enzymatic mode of xylanase and α-L-arabinofuranosidase (**A**) and the value of G' (**B**) and tan δ (**C**) of 0.8% (w/v) samples in water with or without enzyme (Xylanase M1: endo-1,4-β-Xylanase M1 from *Trichoderma viride*, Arabinofuranosidase SE: α-L-Arabinofuranosidase from *Aspergillus nidulan*s)

**Table 1**. Monosaccharides analysis of three arabinoxylan fractions

| No. | Residues | Mol% | | |
|---|---|---|---|---|
| | | CW fraction | HW fraction | KOH fraction |
| 1 | Rhamnose | 15.1±0.3 | ND [a] | ND |
| 2 | Arabinose | 12.3±0.2 | 22.2±0.8 | 24.2±0.6 |
| 3 | Galactose | 3.8±0.1 | 3.7±0.1 | 3.8±0.1 |
| 4 | Glucose | 0.4±0.0 | ND | 0.6±0.1 |
| 5 | Xylose | 58.2±1.9 | 73.7±1.0 | 71.0±0.8 |
| 6 | Galacturonic acid | 9.7±2.2 | 0.4±0.2 | 0.4±0.1 |
| 7 | Glucuronic acid | 0.6±0.1 | ND | ND |

a: ND stands for "none detected". Each experiment was conducted in triplicate to generate a mean and standard deviation.

**Table 2**. Linkage analysis of three arabinoxylan fractions

| No. | Linkages | Mol% | | |
|---|---|---|---|---|
| | | CW fraction | HW fraction | KOH fraction |
| 1 | t-Rha*p* | 0.8±0.0 | ND [a] | ND |
| 2 | 1,2-Rha*p* | 14.2±1.0 | Trace [b] | Trace |
| 3 | t-GlcA*p* | 0.6±0.1 | ND | ND |
| 4 | t-GalA*p* | 0.4±0.1 | ND | ND |
| 5 | 1,4-GalA*p* | 18.7±1.7 | Trace | Trace |
| 6 | 1,4-Glc*p* | 0.3±0.0 | Trace | 0.3±0.1 |
| 7 | t-Gal*p* | 0.6±0.1 | 0.8±0.2 | 0.6±0.0 |
| 8 | t-Ara*f* | 10.0±0.4 | 20.1±1.5 | 18.5±1.7 |
| 9 | 1,3-Ara*f* | 1.5±0.2 | 6.2±0.4 | 8.2±0.4 |
| 10 | t-Xyl*p* | 18.9±1.7 | 23.0±0.7 | 23.2±1.9 |
| 11 | 1,3-Xyl*p* | 10.0±0.1 | 15.6±0.4 | 13.3±0.3 |
| 12 | 1,4-Xyl*p* | 2.7±0.1 | 2.5±0.2 | 3.4±0.3 |
| 13 | 1,2,4-Xyl*p*+1,3,4-Xyl*p* | 16.4±1.5 | 27.0±1.0 | 28.6±0.9 |
| 14 | 1,2,3,4-Xyl*p* | 5.0±0.4 | 4.8±0.5 | 3.9±0.2 |

a: ND stands for "none detected". Trace b means "Mol % < 0.2". Each experiment was conducted in triplicate to generate a mean and standard deviation.

**Table 3**. Parameters of molecular weight and shape of three arabinoxylan fractions

|  | CW fraction | HW fraction | KOH fraction |
|---|---|---|---|
| Intrinsic viscosity ([η], dL/g) [a] | 3.1 | 5.6 | 7.4 |
| Overlap concentration ($c^*$, g/dL) [a] | 0.3 | 0.2 | 0.1 |
| Calculated hydrodynamic radius from [η] ($R_{[\eta]}$, nm) [a] | 38 | 44 | 48 |
| DLS radius ($R_{DLS}$, nm) [b] | 59[d] | 43 | 46 |
| Hydrodynamic radius ($R_h$, nm) [c] | 35 | 42 | 45 |
| Radius of gyration ($R_g$, nm) [c] | 40 | 51 | 43 |
| Weight average molecular weight ($M_W$, kDa) [c] | 1085 | 971 | 953 |
| Number average molecular weight ($M_n$, kDa) [c] | 841 | 640 | 648 |
| Polydispersity Index ($M_W / M_n$) [c] | 1.3 | 1.5 | 1.5 |
| Recovery rate (%) [c] | 85% | 82% | 84% |

a: Measured by capillary viscometer or rheometer (in 0.2M KOH at 25 °C), b: Measured by DLS (in 0.2M KOH at 25°C), c: Measured by HPSEC-MALs system (in 0.04M KOH at 50 °C). d: We note some level of disparity in the $R_h$ estimated using different methods for the CW fraction that contains charged RG-I. This may arise from the differences in ionic strength of solutions used in each of the methods.